Statistics and Its Interface Volume 9 (2016) 365–374

Comparing the second-order properties of spatial point processes

Azam Saadatjouy and Ali Reza Taheriyoun*

Comparing the structural interactions of points in two independent stationary point patterns is as important as comparing the first-order properties or briefly their corresponding intensities. In the present study, three methods based on asymptotic distribution of the periodograms are proposed to test the equality of spectral densities of two independent stationary point processes. In the first method, the sample quantiles of the periodograms ratios are simply used and compared with the exact quantiles under the assumption of the equality of spectral densities. In the second method, a conditional likelihood ratio test is constructed, and the same idea of the first method is used to propose a Bayesian test for the ratio of the spectral density functions. The empirical powers and the empirical type I errors of the tests are also compared in a simulation study. The results emphasize the considerable powers of the tests and the empirical probability of type I errors is very close to the nominal level. Finally, the proposed methods are investigated by using two practical datasets: 1) comparing the locations of capillaries in healthy and cancerous prostate tissue sections and 2) comparing the locations of Alnus trees in two disjoint regions of Iran; both the regions in each dataset are almost of the same identical intensities. The same intensities leads to discovering of the treatment effect (cancer in the first data and location in the second data) in the second-order properties of point patterns.

AMS 2000 subject classifications: Primary 60G55, 62M15; secondary 62F15.
Keywords and phrases: Complete covariance density function, Periodogram, Second-order intensity function, Spatial point process, Spectral density function.

1. INTRODUCTION

1.1 General aspects

Simply speaking, a point pattern as a realization of a point process is a set of points in a window where practically the number of points and their positions are random. There are many observations in the form of point patterns in nature; for instance, the positions of trees in a forest, locations of animal nests, centers of earthquakes, and galaxies in the universe. The analysis of the structure of a point process is strongly related to the variation of points and interaction between two arbitrary points. Interaction as a second order property is usually measured by: 1) the covariance matrix of the positions coordinates of two arbitrary points and 2) the covariance of the number of points in two arbitrary regions. These second-order properties are usually studied by looking at the semi-variogram in the time domain or the spectral density function in the frequency domain [10].

One may be interested in the geometric structures of point patterns and the distribution of the number or locations of the points. These structures depend on both the aggregation and interaction between points. The aggregation and interaction are characterized by intensity and covariance density functions, respectively. Spectral density is the Fourier transform of the complete covariance density function and is estimated asymptotically unbiased with the discrete Fourier transform or periodogram. For a stationary Poisson point process, the spectral density is only a function of the intensity, whereas for the other stationary processes, it is a function of both intensity and the Fourier transform of the covariance density function. Therefore, it is expected that the differences in the spectral density functions of two stationary point processes are attributed to the differences in the intensities and/or complete covariance densities. As a result, if the intensity functions are equal, the source of differences in the spectral densities is the differences among the covariance densities. This is the main idea of this study in testing the equality of the second-order properties of two point processes. Consequently, to distinguish two stationary point processes from each other, first the equality of the intensities is examined [see 4]. If there is no evidence to reject the equality of the intensities, then the second-order properties are examined by testing the equality of the covariance density functions.

Generally, the joint distribution of the periodograms of two point patterns, X and Y, is first reviewed on the Fourier frequencies, respectively denoted by $I_X(\boldsymbol{\omega})$ and $I_Y(\boldsymbol{\omega})$, as intrinsic estimators of the spectral densities at the same frequencies, $\mathrm{f}_X(\boldsymbol{\omega})$ and $\mathrm{f}_Y(\boldsymbol{\omega})$. The asymptotic behavior of the periodograms requires more attention to the geometry of the window. In fact, the effect of the geometry of window has been eliminated before the presentation of the results as described by [2]. Under some regularity conditions, the periodograms are approximately independent and $I_X(\cdot)$ and $I_Y(\cdot)$ are distributed according to a scale family of density functions where the scale parameters are respectively $\mathrm{f}_X(\cdot)$

*Corresponding author.

and $f_Y(\cdot)$. In the first method, this concept is used to determine the significance of the differences in $I_X(\cdot)$ and $I_Y(\cdot)$.

Based on the asymptotic distribution of periodograms, a parametric problem is formulated with observations $I_X(\cdot)$ and $I_Y(\cdot)$ and parameters $f_X(\cdot)$ and $f_Y(\cdot)$ only at the Fourier frequencies. This allows the consideration of likelihood ratio test conditional to the number of points in each point pattern. When there is a likelihood function, it is sufficient to introduce an appropriate prior distribution for the parameters to achieve *a* posteriori properties of the parameters. This concept is considered in our third method.

The spectral analysis of point patterns was first introduced by Bartlett [3]. The technique has been studied and extended to two-dimensional point patterns by [23, 24]. It has also been extended to the spatial and bivariate point processes in [19, 20]. In time series problems, Diggle [8, 9] and Coates and Diggle [5] initiated the modeling of the spectral ratios and accordingly introduced a nonparametric test for the equality of two spectral density functions. Fan and Zhang [11] proposed a regression model for the logarithm of periodograms. They employed a generalized likelihood ratio test to investigate whether a spectral density of a stationary time series belonged to a particular parametric family or not. Similarly, a test based on a Cramer-von-Mises functional type test for a regression model of the logarithm of periodograms was proposed in [6]. To link all the spectral densities simultaneously, a semi-parametric log-linear model for the ratio of spectral density functions was introduced by [12]. They also conducted a test on spectral densities equality for various independent and stationary time series. Lund *et al.* [15] introduced various tests based on the ratios of periodograms and a Bartlett type test for comparing the covariance function of two independent stationary time series. In the present study, three different methods are proposed for testing the equality of the spectral densities of two independent and stationary point processes.

The organization of the present paper is in the following pattern: In continuation of this section, two practical datasets of interest are introduced, that is, the prostate tissues dataset and Alnus trees, motivating the use of proposed tests. Then, the theory of the spectral analysis of spatial point process is briefly reviewed in Section 2. A schematic and a likelihood ratio test are presented in Section 3. This section also contains a Bayesian testing procedure by considering a proper prior distribution for the spectrum of point process. Moreover, the tests are also examined and compared using a simulation study in Section 4. Finally, these methods on both datasets are examined.

1.2 Data and motivations

Two motivating datasets are employed which have led to the main question of this paper in our mind. The first is the location of capillary profiles on a section of prostate tissue. Figure 1 shows the midpoints of the capillaries in sections of healthy and cancerous prostate tissues. The original

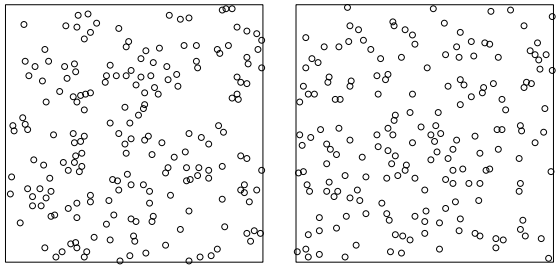

(a) healthy prostate tissue (b) cancerous prostate tissue

Figure 1. The locations of 196 *capillaries on a section of a healthy prostate (a) and the locations of* 185 *capillaries at the same section from a cancerous prostate (b).*

data were observed on a rectangular visual field consisting of 1240×1000 pixels, corresponding to $1860 \times 1500 \mu m$ at the level of the specimen. The coordinates of the capillaries were captured from the rescaled point patterns reported by [13]. From the viewpoint of spatial point process, the data has been studied by [16, 17] and [13], who confirmed that the model of healthy tissue is different from the cancerous one.

The second dataset is devoted to a new data concerning Alnus trees in a forest. After finding out the tragedy of huge illegal logging of the Alnus trees in the Kheyroud forest at the North of Iran, the government decided to artificially reconstruct the forest by planting these trees. The reconstruction has a great importance because of the main role of Alnus trees in the ecosystem of this region, and therefore, it is very important to keep the natural structure of the positions of the trees in the new reconstruction. There are many factors involved in the structure of the positions of trees in nature, e.g., light competition, the distribution of pests, and the slope of the ground. The first factor increases the idea of homogeneity of the positions of trees; while the other factors induce the local effects, and hence, one may be interested in studying the local effect by comparing two totally disjoint regions which are the habitats of this tree. Figure 2 shows the locations of 1586 and 1592 Alnus trees in two locally different regions in rectangular windows whose vertices are located at the geographic coordinates $(555930, 4046300)$ and $(556215, 4046585)$ for the first window and $(556215, 4046300)$ and $(556500, 4046585)$ for the second window. The regions have the same latitude but different longitude. The sampling windows are rescaled on two disjoint square windows with one vertex on the origin and the other vertex is located on $(285, 285)$. This dataset refer to Alnus data, while the point patterns of the first and second regions are respectively denoted by x and y. Generally, in the whole of this paper, the capital words, X and Y represent two independent point processes and the lower cases x and y represent the corresponding observed point patterns. According to the assumption of stationarity, the unbiased estimation of the intensities leads to almost similar

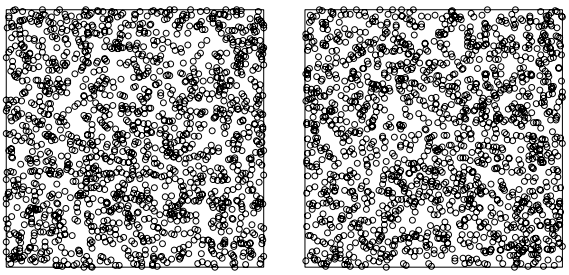

(a) x (b) y

Figure 2. The location of 1586 *(point pattern* x*) and* 1592 *(point pattern* y*) Alnus trees in* $[0, 285] \times [0, 285]$ *windows.*

values, that is, $1586/(285 \times 285) \approx 1592/(285 \times 285)$. Under the consistency of the other effects and due to the same intensities, the treatment effect of longitude could be traced by comparing the interaction of points within two regions. Further discussion on the data is given in Section 4.2.

2. PRELIMINARIES: NOTATIONS AND ASSUMPTIONS

Let N_{lf} be the set of all point patterns and $\mathcal{N}_{lf}$ be a σ-field generated by the subsets of N_{lf}. Formally, a point process is a measurable function $X : (\Omega, \mathcal{F}) \longrightarrow (N_{lf}, \mathcal{N}_{lf})$, where Ω is the sample space and $\mathcal{F}$ is the interested σ-field of Ω. It is often possible to discriminate several spatial point processes by comparing their first- and second-order properties. The first-order property, namely intensity function, is a precise measure of uniformity. It is defined as the expected number of points per unit volume [7, p. 43] as follows:

$$\lambda_X(\mathbf{a}) = \lim_{|\mathrm{d}\mathbf{a}| \to 0} \frac{E[N_X(\mathrm{d}\mathbf{a})]}{|\mathrm{d}\mathbf{a}|}, \qquad \mathbf{a} \in \mathbb{R}^d,$$

where $d \in \mathbb{N}$, $\mathrm{d}\mathbf{a}$ is the small region around the point $\mathbf{a}$, $|\mathrm{d}\mathbf{a}|$ is the volume of this region, and $N_X(\mathrm{d}\mathbf{a})$ is the the number of points of X in this small region. Intensity function is often referred to as the power of point process to create points in a special region. Therefore, a point process is homogeneous or stationary if the intensity function is a constant function. This definition itself explains the way of computing sample intensities in Alnus data.

The second-order characteristic measures the covariance between the number of points of two different regions in an informal manner. We refer to the second-order characteristic by means of second-order intensity function. This function is a measure of the dependency structure of the events [7, p. 43] as follows:

$$\lambda_{XX}(\mathbf{a}, \mathbf{b}) = \lim_{|\mathrm{d}\mathbf{a}|, |\mathrm{d}\mathbf{b}| \to 0} \frac{E[N_X(\mathrm{d}\mathbf{a}) N_X(\mathrm{d}\mathbf{b})]}{|\mathrm{d}\mathbf{a}||\mathrm{d}\mathbf{b}|},$$

for any $\mathbf{a}, \mathbf{b} \in \mathbb{R}^d$ such that $\mathbf{a} \neq \mathbf{b}$. Another important second-order characteristic of a spatial point process is the pair correlation function which is produced from the second-order intensity function by [18, p. 30]

$$g_{XX}(\mathbf{a}, \mathbf{b}) = \frac{\lambda_{XX}(\mathbf{a}, \mathbf{b})}{\lambda_X(\mathbf{a})\lambda_X(\mathbf{b})}.$$

Bartlett [3] proposed the unit-free complete covariance density function, κ_{XX}, that is

$$\begin{aligned} \kappa_{XX}(\mathbf{a}, \mathbf{b}) &= \lambda_X(\mathbf{a})\delta(a_1 - b_1)\delta(a_2 - b_2)\ldots\delta(a_d - b_d) \\ &+ \gamma_{XX}(\mathbf{a}, \mathbf{b}), \end{aligned}$$

where $\delta(a)$ is the Dirac delta function and γ_{XX} is the covariance density function, which in turn can be defined by

$$\begin{aligned} \gamma_{XX}(\mathbf{a}, \mathbf{b}) &= \lim_{|\mathrm{d}\mathbf{a}|, |\mathrm{d}\mathbf{b}| \to 0} (|\mathrm{d}\mathbf{a}||\mathrm{d}\mathbf{b}|)^{-1} \\ &\times E\left[(N_X(\mathrm{d}\mathbf{a}) - \lambda_X(\mathrm{d}\mathbf{a}))\,(N_X(\mathrm{d}\mathbf{b}) - \lambda_X(\mathrm{d}\mathbf{b}))\right] \\ &= \lambda_{XX}(\mathbf{a}, \mathbf{b}) - \lambda_X(\mathbf{a})\lambda_X(\mathbf{b}) \\ &= \lambda_X(\mathbf{a})\lambda_X(\mathbf{b})(g_{XX}(\mathbf{a}, \mathbf{b}) - 1). \end{aligned}$$

Thus, for the stationary point process X with $\lambda_X(\mathbf{a}) = \lambda$, we have $\lambda_{XX}(\mathbf{a}, \mathbf{b}) = \lambda_{XX}(\mathbf{a} - \mathbf{b})$. This equation means that the second-order intensity depends only on the lag vector, $\mathbf{h} = \mathbf{a} - \mathbf{b}$. Moreover, the process is called isotropic if such dependency is an exclusive function of the scalar length, $\|\mathbf{h}\|$, regardless of the orientation of $\mathbf{h}$. Consequently, the complete covariance density function of a stationary point process could be reduced to the following equation:

$$\begin{aligned} \kappa_{XX}(\mathbf{h}) &= \lambda\delta(h_1)\delta(h_2)\ldots\delta(h_d) + \gamma_{XX}(\mathbf{h}) \\ &= \lambda\delta(h_1)\delta(h_2)\ldots\delta(h_d) + \lambda^2(g_{XX}(\mathbf{h}) - 1). \end{aligned}$$

This means that the different interactions may be observed in two point processes with the same intensities. This is a good reason to focus on the comparison of the second-order characteristics instead of the simple intensities of two point patterns. The sample pair correlation functions of x and y in Alnus data are shown in Figure 3. There are some differences in the estimated pair correlation functions of two disjoint windows of Alnus trees. Particularly, for $r = 15, 18, 28, 33, 53, 60,$ and 68, the differences are more visible. This makes us somehow worry about the effect of longitude on the interactions of the Alnus trees; because trees competitions and consequently the planting procedure depend on the longitude and it cannot be simulated using a simple stationary Poisson model. We hope to find a testing approach to enhance the results of plots and move from the intuitive inference to an inference in a mathematical framework.

Although the interpretations of results in the time domain are more objective, just like the time series analysis in both parametric and nonparametric problems, the convergence of algorithms are faster in the frequency domain. Moreover, the spectral representation is more understandable in literature of physics and engineering. The characterization of the spectral density function of the point process

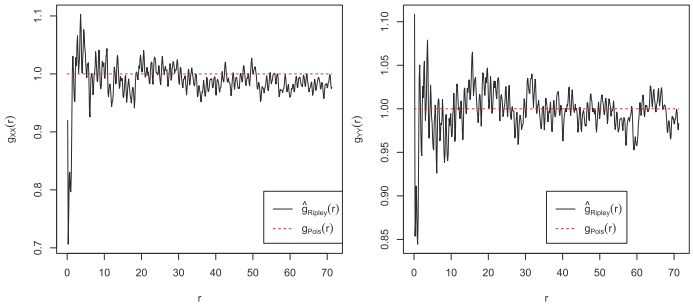

(a) The sample pair correlation function of x (b) The sample pair correlation function of y

Figure 3. Estimated pair correlation function, $g(r)$, of Alnus data and the theoretical value of $g(r)$ for a Poisson process.

X, is denoted by f_X and is obtained from the Fourier transform of the complete covariance density function. Under the stationarity assumption, we have

$$\begin{aligned}\mathrm{f}_X(\boldsymbol{\omega}) &= \int_{\mathbb{R}^d} \kappa_{XX}(\mathbf{h}) e^{-i\langle\boldsymbol{\omega},\mathbf{h}\rangle} \mathrm{d}\mathbf{h} \\ &= \int_{\mathbb{R}^d} [\lambda_X \delta(h_1)\delta(h_2)\ldots\delta(h_d) + \lambda_X^2 \left(g_{XX}(\mathbf{h}) - 1\right)] \\ &\qquad e^{-i\langle\boldsymbol{\omega},\mathbf{h}\rangle} \mathrm{d}\mathbf{h} \\ &= \lambda_X + \lambda_X^2 \int_{\mathbb{R}^d} \left(g_{XX}(\mathbf{h}) - 1\right) e^{-i\langle\boldsymbol{\omega},\mathbf{h}\rangle} \mathrm{d}\mathbf{h}.\end{aligned}$$

For stationary Poisson point processes, since $g_{XX} \equiv 1$ [18, p. 30], thus $\mathrm{f}_X(\boldsymbol{\omega}) = \lambda_X$.

Suppose that a point pattern contains n_X points in a rectangular window, W, with sides of length l_i along the i'th coordinate of the Cartesian system for $i = 1, \ldots, d$, and let $\mathbf{z}_j$, $j = 1, ..., n_X$, be the positions of the points. Note also that n_X is an observation from the random variable $N_X(W)$. Spectral density function is estimated using the discrete Fourier transform of the sample complete covariance density function. The estimated function is called periodogram and evaluated at the Fourier frequencies $\boldsymbol{\omega}_\mathbf{p} = 2\pi\mathbf{p}$, where $\mathbf{p} = (p_1, \ldots, p_d)$, $p_j \in \{-n_X, \ldots, n_X\}$ and $j = 1, \ldots, d$. The values of periodogram show the relative proportion of every frequency $\boldsymbol{\omega}$ to the total spatial variance of the process [14]. Formally, the periodogram is defined by

$$\begin{aligned}I_X(\boldsymbol{\omega}) &= F_X(\boldsymbol{\omega})\overline{F_X}(\boldsymbol{\omega}) \\ &= \left(\sum_{j=1}^{n_X} exp\{i\boldsymbol{\omega}^T L^{-1}\mathbf{z}_j\}\right)\left(\sum_{k=1}^{n_X} exp\{-i\boldsymbol{\omega}^T L^{-1}\mathbf{z}_k\}\right) \\ &= \sum_{j=1}^{n_X}\sum_{k=1}^{n_X} exp\{i\boldsymbol{\omega}^T L^{-1}(\mathbf{z}_j - \mathbf{z}_k)\} \\ &= \sum_{j=1}^{n_X}\sum_{k=1}^{n_X} exp\{i\boldsymbol{\omega}^T L^{-1}\mathbf{h}_{jk}\},\end{aligned}$$

where $\overline{F_X}(\boldsymbol{\omega})$ is the complex conjugate of $F_X(\boldsymbol{\omega})$, and L is a scaling matrix constructed as $L = diag(l_1, \ldots, l_d)$. Note that $L^{-1}\mathbf{z}_j$ precisely scales the window W to the unite cube.

The periodogram is an asymptotic unbiased but inconsistent estimate of the spectral density function at the Fourier frequencies. The spectral density, $\mathrm{f}_X(\boldsymbol{\omega})$, tends to zero as $\|\boldsymbol{\omega}\| \to \infty$. Thus, when $n_X < 100$, it is recommended to compute the periodogram only for $\mathbf{p} \in \{0, \pm1, \ldots, \pm16\}^d$ [20]. The symmetric behavior of periodogram, i.e. $I_X(\boldsymbol{\omega}_\mathbf{p}) = I_X(\boldsymbol{\omega}_{-\mathbf{p}})$, halves the cost of computation. To compare the spectral densities of two point processes in our simulation study, the set of Fourier frequencies is considered as $\mathbf{p} \in \{\pm1, \ldots, \pm8\}^d = \mathbb{P}$.

Pagano [22] confirmed that the periodogram of a realization of a 2-dimensional stationary random field is asymptotically distributed as the exponential distribution and the results were extended to higher dimensions in [26]. Using the same method and given $N_X(W) = n_X$, similar results were obtained for d-dimensional point processes:

$$\frac{2I_X(\boldsymbol{\omega}_\mathbf{p})}{\mathrm{f}_X(\boldsymbol{\omega}_\mathbf{p})} \sim \chi^2_{(2)}, \qquad \boldsymbol{\omega}_\mathbf{p} \neq \mathbf{0}, \tag{1}$$

and

$$\frac{2\{I_X(\mathbf{0}) - \lambda_\mathbf{X}\}}{\mathrm{f}_X(\mathbf{0})} \sim \chi^2_{(1)}.$$

The periodograms are asymptotically independent under mild restrictions on the geometry of the window, W. Precisely, Bandyopadhyay and Lahiri [2] showed that the periodograms are independent when W is a cube in $\mathbb{R}^d$. The independence does not necessarily hold for the general shape of W, e.g. spheres and hyper-rectangles and the general sampling designs.

3. TESTING APPROACHES

In this section, we introduce three testing procedures based on the asymptotic distribution of periodograms to compare the spectral densities of two independent and stationary point processes in $\mathbb{R}^d$. Suppose that X and Y are independent stationary point processes and let I_X, f_X, I_Y, and f_Y be their corresponding periodograms and spectral density functions, respectively. To compare the second-order properties of X and Y, we need to test

$$H_0 : \mathrm{f}_X(\boldsymbol{\omega}) = \mathrm{f}_Y(\boldsymbol{\omega}), \text{ versus } H_1 : \mathrm{f}_X(\boldsymbol{\omega}) \neq \mathrm{f}_Y(\boldsymbol{\omega}), \tag{2}$$

for any $\boldsymbol{\omega} \in \mathbb{R}^d$ and thus the problem is nonparametric.

A rejection area for (2) is constructed based on the periodograms only at the Fourier frequencies. Using (1) and the asymptotic independence of I_X and I_Y, and conditioning on $N_X(W) = n_X$, and $N_Y(W) = n_Y$, we obtain that

$$\left.\frac{I_X(\boldsymbol{\omega}_\mathbf{p})/\mathrm{f}_X(\boldsymbol{\omega}_\mathbf{p})}{I_Y(\boldsymbol{\omega}_\mathbf{p})/\mathrm{f}_Y(\boldsymbol{\omega}_\mathbf{p})}\right| (N_X(W) = n_X, N_Y(W) = n_Y) \sim F(2,2).$$

Thus, the asymptotic conditional distribution of $T(\mathbf{p}) = I_X(\boldsymbol{\omega}_\mathbf{p})/I_Y(\boldsymbol{\omega}_\mathbf{p})$ under H_i is

$$f_{T(\mathbf{p})|N_X,N_Y}(t|n_x,n_y) = \frac{\eta_{i\mathbf{p}}}{(\eta_{i\mathbf{p}}+t)^2}, \quad t>0, \tag{3}$$

where $\eta_{0\mathbf{p}} = 1$ and $\eta_{1\mathbf{p}} = \mathrm{f}_X(\boldsymbol{\omega}_\mathbf{p})/\mathrm{f}_Y(\boldsymbol{\omega}_\mathbf{p})$. Note that under the null hypothesis, $T(\mathbf{p})$ is conditionally distributed as $F(2,2)$. We are now ready to introduce the rejection area.

3.1 Schematic approach

Using (3), one may test the hypotheses (2) by looking at the $Q-Q$ plot of $T(\mathbf{p})$. Therefore, the level of researcher's consent plays an important role in decision making and the rejection criterion changes from person to person. Considering the distribution of the ratios of periodograms under H_0, one may build a goodness-of-fit test based on the sample quantiles. Under the null, the number of $T(\mathbf{p})$'s exceeding a given threshold u, T_{num} say, is distributed as a binomial random variable with $|\mathbb{P}|_C$ trials and the approximately success probability

$$p = P(T(\mathbf{p})>u) = \frac{1}{1+u},$$

where $|A|_C$ denotes the cardinality of A. Thus, using the normal approximation, one may reject H_0 at the significance level, α, when

$$\left|(T_{\text{num}} - |\mathbb{P}|_C p)/\sqrt{|\mathbb{P}|_C p(1-p)}\right| > z_{\alpha/2}.$$

The expected value of a random variable with density function (3) does not exist and consequently it is not possible to employ the central limit theorem on $T(\mathbf{p}), \mathbf{p}\in\mathbb{P}$. We then follow the same method as [5] and define $R(\mathbf{p}) = \ln(I_X(\boldsymbol{\omega}_\mathbf{p})) - \ln(I_Y(\boldsymbol{\omega}_\mathbf{p}))$. Under the null hypothesis and given $N_X(W)=n_X$ and $N_Y(W)=n_Y$, the statistic $R(\mathbf{p})$ is conditionally distributed as a logistic random variable with distribution function

$$F_R(r) = \frac{1}{1+e^{-r}}, \quad -\infty<r<\infty.$$

Thus, one can consider the sample average of squared deviations as

$$\overline{R} = \frac{1}{|\mathbb{P}|_C}\sum_{\mathbf{p}} R^2(\mathbf{p})$$

and reject H_0 for large enough values of $\overline{R}$. It could be verified that $E[R^2(\mathbf{p})] = \pi^2/3$ and $Var(R^2(\mathbf{p})) = 16\pi^4/45$. So, using the normal approximation, the null is rejected at level α when

$$\left|\frac{\overline{R}-\pi^2/3}{\sqrt{16\pi^4/(45\times|\mathbb{P}|_C)}}\right| > z_{\alpha/2}.$$

The other goodness-of-fit tests such as Kolmogorov-Smirnov can be applied to this problem as well.

3.2 Conditional likelihood ratio test (CLRT)

Let us denote the vector of periodograms $I_X(\boldsymbol{\omega}_\mathbf{p})$ and the vector of spectral densities $\mathrm{f}_X(\boldsymbol{\omega}_\mathbf{p})$, $\mathbf{p}\in\mathbb{P}$, by $\mathbf{I}_X$ and $\mathbf{f}_X$, respectively, and use the same notations to define $\mathbf{I}_Y$ and $\mathbf{f}_Y$. The asymptotic independence and the asymptotic distribution of periodograms are used to compute the density function of the random vector $(\mathbf{I}_X,\mathbf{I}_Y)$ and hence the conditional likelihood function in terms of the periodograms. Thus, the asymptotic conditional likelihood function given $N_X(W)=n_X$ and $N_Y(W)=n_Y$ for large number of points is

$$L(\mathbf{f}_X,\mathbf{f}_Y|\mathbf{I}_X,\mathbf{I}_Y) = \prod_{\mathbf{p}} \frac{\exp\left(-\frac{I_X(\boldsymbol{\omega}_\mathbf{p})}{\mathrm{f}_X(\boldsymbol{\omega}_\mathbf{p})} - \frac{I_Y(\boldsymbol{\omega}_\mathbf{p})}{\mathrm{f}_Y(\boldsymbol{\omega}_\mathbf{p})}\right)}{\mathrm{f}_X(\boldsymbol{\omega}_\mathbf{p})\mathrm{f}_Y(\boldsymbol{\omega}_\mathbf{p})}.$$

The third rejection area for (2) is obtained by comparing the conditional likelihoods under the null and the alternative hypotheses. Let $L_{H_i|N_X,N_Y}(\mathbf{f}_X,\mathbf{f}_Y|\mathbf{I}_X,\mathbf{I}_Y)$, $i=1,2$, be the conditional likelihoods under H_i given the fixed number of observations $N_X(W)=n_X$ and $N_Y(W)=n_Y$. Let also Θ_i denote the parameter space under H_i, $i=1,2$. Thus, the small value of the conditional likelihood ratio

$$\Lambda = \frac{\max_{\Theta_0} L_{H_0|N_X,N_Y}(\mathbf{f}_X,\mathbf{f}_Y|\mathbf{I}_X,\mathbf{I}_Y)}{\max_{\Theta_1} L_{H_1|N_X,N_Y}(\mathbf{f}_X,\mathbf{f}_Y|\mathbf{I}_X,\mathbf{I}_Y)},$$

encourages the rejection of H_0. In other words, we reject the null when $\Lambda<c_\alpha$ where c_α is determined in such a way that the level of test does not exceed α. The conditional ML estimates under H_1 are

$$\widehat{\mathrm{f}}_X(\boldsymbol{\omega}_\mathbf{p}) = I_X(\boldsymbol{\omega}_\mathbf{p}) \quad \text{and} \quad \widehat{\mathrm{f}}_Y(\boldsymbol{\omega}_\mathbf{p}) = I_Y(\boldsymbol{\omega}_\mathbf{p}),$$

and under the null hypothesis the conditional ML estimates of $\mathrm{f}_X(\boldsymbol{\omega}_\mathbf{p}) = \mathrm{f}_Y(\boldsymbol{\omega}_\mathbf{p})$ are $(I_X(\boldsymbol{\omega}_\mathbf{p}) + I_Y(\boldsymbol{\omega}_\mathbf{p}))/2$, for $\mathbf{p}\in\mathbb{P}$. Thus, the rejection area is changed to

$$\Lambda = \prod_{\mathbf{p}} \frac{4I_X(\boldsymbol{\omega}_\mathbf{p})I_Y(\boldsymbol{\omega}_\mathbf{p})}{(I_X(\boldsymbol{\omega}_\mathbf{p})+I_Y(\boldsymbol{\omega}_\mathbf{p}))^2} < c_\alpha,$$

or equivalently

$$\ln(\Lambda) = \sum_{\mathbf{p}} \ln\left(\frac{4I_X(\boldsymbol{\omega}_\mathbf{p})I_Y(\boldsymbol{\omega}_\mathbf{p})}{(I_X(\boldsymbol{\omega}_\mathbf{p})+I_Y(\boldsymbol{\omega}_\mathbf{p}))^2}\right) < c'_\alpha, \tag{4}$$

for a suitable choice of c'_α. Under the null hypothesis the random variables $\ln\left(4I_X(\boldsymbol{\omega}_\mathbf{p})I_Y(\boldsymbol{\omega}_\mathbf{p})/(I_X(\boldsymbol{\omega}_\mathbf{p})+I_Y(\boldsymbol{\omega}_\mathbf{p}))^2\right)$, $\mathbf{p}\in\mathbb{P}$, are independently and identically distributed as $Z = \ln\left(4T_1T_2/(T_1+T_2)^2\right)$ where T_1 and T_2 are independent exponentially distributed random variables with unit mean. It was computed in [15] that $E[Z] = \ln(4)-2 \approx -0.614$ and $var(Z) = 4-\pi^2/3+(4-8\gamma+2\gamma^2) \approx 0.759$, where $\gamma\approx 0.577$ is the Euler's constant. For large values of $|\mathbb{P}|_C$ the central limit theorem features the rejection area as

$$\frac{\ln(\Lambda) - |\mathbb{P}|_C E[Z]}{\sqrt{|\mathbb{P}|_C var(Z)}} < z_{1-\alpha}.$$

According to the cost of sampling, in some problems the sample sizes N_X and N_Y are supposed to be fixed numbers, called again n_X and n_Y. Under the assumption of constant sample size, the CLRT is also a likelihood ratio test and all the features of likelihood ratio test including the χ^2 approximation are accessible.

3.3 Bayesian approach

This approach is discussed only for the case of constant sample size. Following [25, p. 231], we compute the Bayes factor, B_{01}^{π}, as the ratio of the likelihood function under the null hypothesis and the marginal density of the periodograms under the alternative, that is

$$\begin{aligned} B_{01}^{\pi} &= \frac{f(\mathbf{I}_X, \mathbf{I}_Y | \mathbf{f}_X = \mathbf{f}_Y)}{m_1(\mathbf{I}_X, \mathbf{I}_Y)} \\ &= \frac{f(\mathbf{I}_X, \mathbf{I}_Y | \mathbf{f}_X = \mathbf{f}_Y)}{\int f(\mathbf{I}_X, \mathbf{I}_Y | \mathbf{f}_X, \mathbf{f}_Y) \pi_1(\mathbf{f}_X, \mathbf{f}_Y) \mathrm{d}\mathbf{f}_X \mathrm{d}\mathbf{f}_Y}, \end{aligned} \tag{5}$$

where the numerator denotes the likelihood under the null hypothesis and $f(\mathbf{I}_X, \mathbf{I}_Y | \mathbf{f}_X, \mathbf{f}_Y)$ and $\pi_1(\mathbf{f}_X, \mathbf{f}_Y)$ represent respectively the likelihood and the prior densities under H_1 [25, p. 231]. Using the vector of ratios $\mathbf{T} = (T(\mathbf{p}), \mathbf{p} \in \mathbb{P})$ instead of the direct use of periodograms, the parameter spaces and hence the priors under the null and the alternative hypotheses are simplified. Note that the parameter space under the null hypothesis is

$$\Theta_0 = \left\{ (\mathbf{f}_X, \mathbf{f}_Y) \in \mathbb{R}_+^{|\mathbb{P}|_C} \times \mathbb{R}_+^{|\mathbb{P}|_C} \middle| \mathbf{f}_X = \mathbf{f}_Y \right\},$$

whereas the distribution of $\mathbf{T}$ under H_0 does not depend on parameters. Particularly, regarding (3), the asymptotic joint density function of $\mathbf{T}$ is

$$f_{\mathbf{T}|H_i}(\mathbf{t}) = \prod_{\mathbf{p} \in \mathbb{P}} \frac{\eta_{i\mathbf{p}}}{(\eta_{i\mathbf{p}} + t_{\mathbf{p}})^2}, \qquad \text{for } \mathbf{t} = (t_{\mathbf{p}}, \mathbf{p} \in \mathbb{P}).$$

We thus compute the Bayes factor for the point null hypothesis $H_0 : \boldsymbol{\eta}_{\mathbf{p}} = \mathbf{f}_X(\mathbf{p}) \oslash \mathbf{f}_Y(\mathbf{p}) = \mathbf{1}$ versus $H_1 : \boldsymbol{\eta}_{\mathbf{p}} \neq \mathbf{1}$ using $\mathbf{T}$, where $\oslash$ is simple component-wise division and $\mathbf{1}$ is a $|\mathbb{P}|_C \times 1$ vector of ones. The Bayes factor for the new testing problem is

$$B_{01}^{\pi} = \frac{f_{\mathbf{T}}(\mathbf{t}|\boldsymbol{\eta} = \mathbf{1})}{m_{\mathbf{T}}(\mathbf{t}|H_1)} = \frac{f_{\mathbf{T}}(\mathbf{t}|\boldsymbol{\eta} = \mathbf{1})}{\int f_{\mathbf{T}}(\mathbf{t}|H_1) \pi_1(\boldsymbol{\eta}) \mathrm{d}\boldsymbol{\eta}}, \tag{6}$$

where $\boldsymbol{\eta} = (\eta_{\mathbf{p}}, \mathbf{p} \in \mathbb{P})$, $m_{\mathbf{T}}(\mathbf{t}|H_1)$ is the marginal density of $\mathbf{T}$ and π_1 is the prior density of $\boldsymbol{\eta}$ under H_1. For the sake of conciseness, we refer to [25, p. 228] for the rejection criterion using the Bayes factor.

We need to introduce a priori distribution under the alternative. Let the elements of the parameter vectors $\mathbf{f}_X$ and $\mathbf{f}_Y$ be independent and $\ln(\mathrm{f}_X(\boldsymbol{\omega}_{\mathbf{p}}))$ and $\ln(\mathrm{f}_Y(\boldsymbol{\omega}_{\mathbf{p}}))$ are independently distributed as $N(\mu_X, \sigma_X^2)$ and $N(\mu_Y, \sigma_Y^2)$, respectively, i.e., the density function of f_X is

$$f_{\mathrm{f}_X}(s) = \frac{1}{s\sqrt{2\pi\sigma_X^2}} \exp\{-\frac{1}{2\sigma_X^2}(\ln s - \mu_X)^2\}, \quad s > 0,$$

for $\mu_X \in \mathbb{R}$ and $\sigma_X > 0$. Hence, the prior distribution of $\eta(\mathbf{p})$ under the alternative hypothesis is Log-normal with parameters $\mu_X - \mu_Y$ and $\sigma_X^2 + \sigma_Y^2$, and the marginal density of $\mathbf{T}$ on H_1 is

$$\begin{aligned} m_{\mathbf{T}}(\mathbf{t}|H_1) = \int_{\mathbb{R}_+^{|\mathbb{P}|_C}} \prod_{\mathbf{p} \in \mathbb{P}} \frac{\eta_{1\mathbf{p}}}{(\eta_{1\mathbf{p}} + t_{\mathbf{p}})^2} \frac{1}{\eta_{1\mathbf{p}}\sqrt{2\pi(\sigma_X^2 + \sigma_Y^2)}} \\ exp\{-\frac{1}{2(\sigma_X^2 + \sigma_Y^2)}(\ln \eta_{1\mathbf{p}} - (\mu_X - \mu_Y))^2\} d\eta_{1\mathbf{p}}, \end{aligned}$$

and consequently the Bayes factor becomes

$$\begin{aligned} B_{10}^{\pi} &= \frac{1}{B_{01}^{\pi}} \\ &= \prod_{\mathbf{p} \in \mathbb{P}} (1 + t_{\mathbf{p}})^2 \int_{\mathbb{R}_+^{|\mathbb{P}|_C}} \prod_{\mathbf{p} \in \mathbb{P}} \frac{1}{(\eta_{1\mathbf{p}} + t_{\mathbf{p}})^2} \frac{1}{\sqrt{2\pi(\sigma_X^2 + \sigma_Y^2)}} \\ &\times \exp\{-\frac{1}{2(\sigma_X^2 + \sigma_Y^2)}(\ln \eta_{1\mathbf{p}} - (\mu_X - \mu_Y))^2\} d\eta_{1\mathbf{p}}. \end{aligned}$$

A numerical study is designed for comparison of the presented approaches in the following section.

4. NUMERICAL RESULTS

4.1 Simulation study

In order to evaluate the performance of the mentioned tests in comparing the spectral density functions of two stationary point processes, three distinct types of point processes were simulated on the square region $W = [0, l] \times [0, l]$. As mentioned earlier, the periodograms at Fourier frequencies are approximately distributed as independent χ^2 random variables as $n_X \to \infty$. Since the results of this study strongly depend on this convergence, the windows and intensities of point processes are chosen in such a way that the number of points achieves an acceptable performance for the convergence. The considered point processes in this simulation study are as follows:

- $P(\lambda)$: Stationary Poisson process with intensity λ,
- $MatC(\kappa, r, \mu)$: Matèrn cluster process with the parent process of $P(\kappa)$, radius parameter of the clusters of r and the mean number of points per cluster of μ,
- $IMat_1(\kappa, r)$: Inhibition process of Matèrn's first type with homogeneous Poisson process of intensity κ for proposal points and the inhibition distance parameter r, i.e., no pair could have an inter-point distance less than r.

Simulated realizations from the employed point patterns are shown in Figure 4. More detailed descriptions of these processes can be found in [1]. In each setting, 1,000 simulation replicates are used. Table 1 shows the ratios of rejections at level $\alpha = 0.05$. The ratio of rejections for two different processes represents the empirical power and the ratios of rejections for the same processes represents the empirical size of the tests. As previously explained, the spectral den-

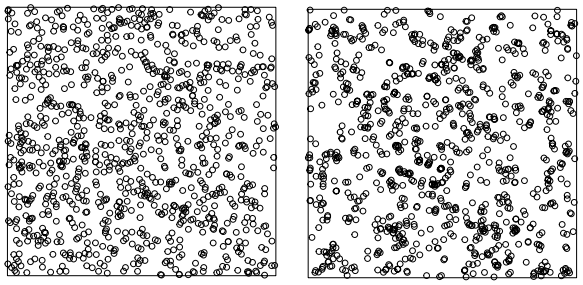

(a) $P(10)$ (b) $MatC(10, 0.1, 1)$

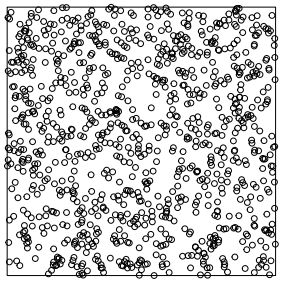

(c) $IMat_1(10, 0.01)$

Figure 4. Realizations of spatial point processes used in the simulation on a 10×10 *region. (a) Poisson process of intensity* $\lambda = 10$*, (b) Matèrn cluster process with* $\kappa = 10$*,* $r = 0.1$ *and* $\mu = 1$ *and (c) Matèrn inhibition process of type* I *with* $\kappa = 10$*,* $r = 0.01$*.*

sity function of stationary Poisson processes is equal to the constant intensity. However, for non Poisson stationary processes, the spectral density is a function of constant intensity. Therefore, since the relative difference of the intensities of processes $P(10)$ and $P(20)$ are the same as $P(100)$ and $P(200)$, hence the same powers are expected for different windows. This claim is confirmed by the simulation study. Moreover, the power of each test increases by growth of the relative difference of intensities.

On the other hand, the window plays a critical role in testing a Poisson process versus a clustered or inhibition processes. For instance, as shown in Table 1, the empirical power of testing $P(\cdot)$ versus $MatC(\cdot, \cdot, \cdot)$ or $IMat_1(\cdot, \cdot)$, in almost all settings, is increasing in the size of window. This is due to the structure of spectral density of the process under H_1 which is not equal to the constant intensity. It is worth mentioning that the main factor affecting the power is the number of points indeed. The result shows that detecting a stationary Poisson process from another non Poisson stationary process needs more samples when compared with the problem of recognition of two stationary Poisson processes. Maybe the rate of convergence in the joint asymptotic distribution of periodograms can explain this in the behavior of tests.

Consider the testing problem of (2) when X is a Poisson process of intensity 100 and Y is $MatC(100, 0.1, 4)$ process. The power of all three testing methods for this setting of parameters produce greater power in comparison with the case when Y is a $MatC(100, 0.1, 1)$ process. Visually, for fixed parameters κ and r, the clustered behavior of Matèrn cluster process is increasing in μ and all tests recognize this behavior. The visual discrimination of $IMat_1(10, 0.2)$ from $IMat_1(10, 0.02)$ is not as simple as the previous case. Both point processes have the same intensities and therefore, the differences originate from the differences in the interaction between the points of each process or simply from different spectral densities. However, the tests show an acceptable power in the recognition of these two processes.

Testing procedures are repeated with two identical processes X and Y to testify the empirical level which we would like to keep at level 0.05. This procedure employs the same processes X and Y from $P(10)$, $MatC(10, 0.05, 4)$, and $IMat_1(10, 0.05)$. Tests based on T_{num}, $\overline{R}$, and CLRT are conservative and they reject the null hypothesis at rates reasonably close to the nominal level, 0.05. The results of Table 1 show that the T_{num} test has the greatest power and relatively the smallest probability of type I error. Informally, for 1,000 simulation replicates from $P(10)$ and assuming values $\mu_X = \mu_Y = 5$ and $\sigma_X^2 = \sigma_Y^2 = 1$ for the hyper parameters, the test based on the Bayes factor rejects the null hypothesis at level less than 0.01.

4.2 Real data

Mattfeldt *et al.* [16, 17] proposed the use of Strauss hard-core model for the locations of capillaries in prostate tissues. The model consists of four parameters, i.e., the intensity parameter, λ, the minimum distance parameter, r_0, the minimum distance of uncorrelated points, R, and the interaction strength, γ. We refer to Baddeley and Turner [1] for Strauss hard-core model. Both results of the studies of [16, 17] confirmed that the difference between healthy and cancerous tissues is the difference in γ parameter of point processes. Hahn [13] verified the difference in the spatial model of healthy and cancerous tissues by testing the corresponding empirical K functions. According to the number of points, both point patterns are assumed to have the same intensities. Thus, the methods described in Section 3 can be employed to test the differences in the complete covariance functions of the capillaries of healthy and cancerous tissues. The *p-values* of tests based on $T_{\text{num}}, \overline{R}$, and CLR statistics are $0.36, 0.25$ and 0.18, respectively, of which all do not reject the hypothesis of the same complete covariance functions. Summing up this result with the result reported by [13], one may claim that cancer does not affect the first and second order properties of the locations of capillaries on the prostate tissue. Thus, the reported difference by [13] is reflected on higher moments.

As mentioned earlier, the second dataset is devoted to two point patterns of Alnus trees, as shown in Figure 2. A summary statistic for X and Y is initiated, called the nearest-neighbor function G [see 18, p. 35]. The sample G functions of x and y along the theoretic G function of the stationary Poisson process are as shown in Figure 5(a) and 5(b).

Table 1. The ratio of rejections for different point processes and different tests

		Testing based on			
	l	T_{num}	$\overline{R}$	CLRT	Bayesian
$P(10)$ vs $P(20)$	1	0.825	0.232	0.331	0.195
	5	0.954	0.160	0.279	0.194
	$\sqrt{40}$	0.961	0.164	0.259	0.285
	$\sqrt{60}$	0.966	0.147	0.250	0.291
	$\sqrt{80}$	0.970	0.168	0.274	0.294
	$\sqrt{100}$	0.956	0.195	0.292	0.291
$P(100)$ vs $P(200)$	1	0.948	0.168	0.278	0.112
	2	0.954	0.176	0.277	0.197
	3	0.954	0.151	0.262	0.201
	5	0.964	0.169	0.269	0.282
	$\sqrt{40}$	0.966	0.162	0.256	0.285
	$\sqrt{60}$	0.971	0.162	0.265	0.279
$P(10)$ vs $P(35)$	5	1.000	0.767	0.899	0.784
	10	1.000	0.753	0.904	0.784
$P(35)$ vs $P(30)$	5	0.167	0.044	0.045	0.100
	10	0.155	0.043	0.057	0.140
$P(35)$ vs $P(50)$	5	0.524	0.067	0.101	0.190
	10	0.506	0.065	0.089	0.210
$P(100)$ vs $MatC(100, 0.1, 1)$	0.5	0.364	0.056	0.071	0.190
	1	0.181	0.056	0.070	0.150
	2	0.342	0.051	0.077	0.120
	3	0.692	0.075	0.136	0.180
	5	0.896	0.114	0.190	0.580
$P(100)$ vs $MatC(100, 0.1, 4)$	0.5	0.999	0.829	0.915	0.843
	1	1.000	0.971	0.993	0.986
	2	1.000	1.000	1.000	1.000
	3	1.000	1.000	1.000	1.000
$P(100)$ vs $MatC(100, 0.05, 4)$	0.5	0.998	0.905	0.955	0.919
	1	1.000	1.000	1.000	1.000
	2	1.000	1.000	1.000	1.000
	3	1.000	1.000	1.000	1.000
$P(100)$ vs $IMat_1(100, 0.05)$	0.5	0.905	0.281	0.385	0.257
	1	0.997	0.444	0.628	0.378
	2	1.000	0.507	0.710	0.493
	3	0.998	0.498	0.671	0.476
	5	1.000	0.509	0.699	0.497
$IMat_1(10, 0.2)$ vs $IMat_1(10, 0.02)$	10	1.000	0.911	0.975	0.948
$IMat_1(10, 0.1)$ vs $IMat_1(10, 0.01)$	10	0.834	0.103	0.155	0.935
$MatC(10, 0.1, 1)$ vs $MatC(10, 0.1, 2)$	10	1.000	0.575	0.754	0.537
$MatC(10, 0.1, 1)$ vs $MatC(10, 0.1, 4)$	10	1.000	1.000	1.000	1.000
$P(10)$ vs $P(10)$	10	0.056	0.042	0.051	0.007
$P(35)$ vs $P(35)$	10	0.050	0.051	0.057	0.007
$IMat_1(10, 0.05)$ vs $IMat_1(10, 0.05)$	10	0.060	0.041	0.044	0.007
$MatC(10, 0.05, 4)$ vs $MatC(10, 0.05, 4)$	10	0.066	0.048	0.053	0.007

Figures 5(c)–5(h) also show the same demonstrations for sample L, K, and F functions and we respectively refer to [18, p. 35, 33 and 35] for the computation of these functions. Although it is typical to employ only one of these statistics, Figure 5 shows the possible disagreements of the decisions based on the global envelopes. Simply speaking, the gray areas of all figures represent the acceptance regions of the stationary Poisson model for data based on the corresponding statistic. The hypothesis of stationary Poisson model is rejected based on a statistic at level $\alpha = 0.05$, when the sample statistic does not remain between the given boundaries at least for a point $r^* \in \mathbb{R}_+$ [see 21, for details]. Comparing the sample G and L functions and the prepared boundaries emphasizes the lack of fitness of stationary Poisson process to both point patterns. Based on sample K function and the corresponding global envelope, the hypothesis of sta-

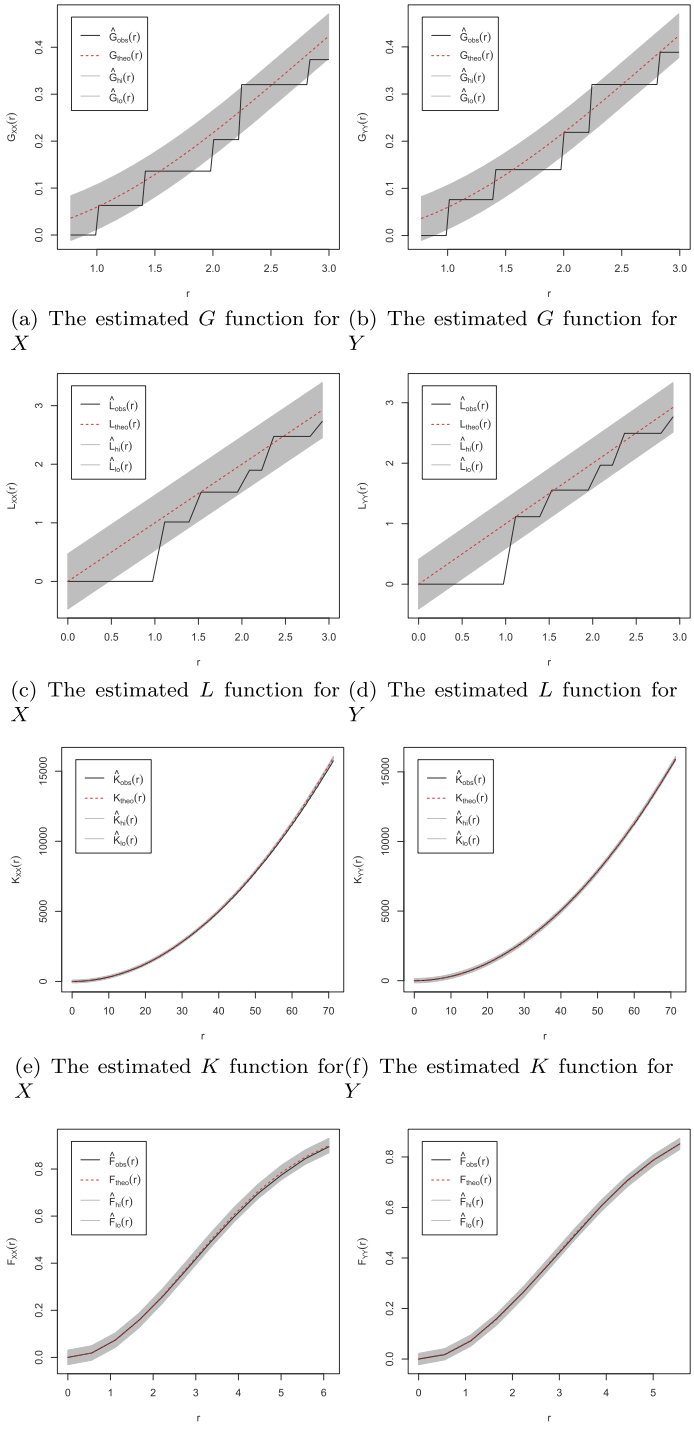

(a) The estimated G function for X (b) The estimated G function for Y

(c) The estimated L function for X (d) The estimated L function for Y

(e) The estimated K function for X (f) The estimated K function for Y

(g) The estimated F function for X (h) The estimated F function for Y

Figure 5. The estimated G, L, K and F functions for Alnus data. The figures also contain the theoretic functions for the stationary Poisson point process and upper and lower boundaries are given for each graph based on the global enveloping of 19 simulations from stationary Poisson process.

tionary Poisson model is rejected for the point pattern x. However, based on F function, one may consider the stationary Poisson model and thus comparing the spectral densities is equivalent to comparing the intensities. These contradictory decisions based on the summary statistics propose that it is not advisable to trust only in a summary statistic and leave the others. Therefore, comparing the stationary intensities to explore the difference between the spectral density functions is misleading for this data. So, we need a testing procedure not depending on the further assumption of stationary Poisson model.

On the other hand, the estimated intensities of both point patterns are very close together and thus the effect of longitude is not traceable within the first order properties. The second-order properties are looked into by testifying the equality of the interactions between points in x and y. The rejection of null hypothesis represents the significance of the effect of longitude on the interactions of the positions of trees. The problem of reconstruction of the forest becomes complicated by the rejection of H_0.

The nonparametric nature of the presented methods helps to solve the problem regardless of any further assumption. Therefore, there is need to test whether the differences in sample pair correlation functions (Figure 3) are significant enough to reject the hypothesis of the same second-order properties or not. These small differences in sample functions are addressed as the treatment effect of longitude in sampling windows. The first order comparison is not helpful since the estimated intensities are very close. The other choice is to compare the second order properties. The *p-value*s corresponding to T_{num}, $\overline{R}$, and CLRT are, respectively 0.584, 0.167, and 0.054, which cannot reject the hypothesis of $H_0 : \mathrm{f}_X = \mathrm{f}_Y$ and thus we claim that the interaction of trees is not affected by the local factor of longitude. As shown in Figure 3, the sample pair correlation functions show the same behavior; they are different in some small intervals, but it is difficult to visually compare them.

ACKNOWLEDGEMENTS

The authors would like to express their gratitude to Professor Rasmus Waagepetersens, whose very kind comments helped improve this work. We are grateful to the anonymous referee for interesting and helpful comments that revolutionary improved the previous version of this paper.

Received 29 March 2015

REFERENCES

[1] Baddeley, A. and Turner, R. (2005). spatstat: An R package for analyzing spatial point patterns. *J. Statist. Software* **12** 1–42.

[2] Bandyopadhyay, S. and Lahiri, S. N. (2009). Asymptotic properties of discrete Fourier transforms for spatial data. *Sankhyā* **71** 221–259. MR2639292

[3] Bartlett, M. (1964). The spectral analysis of two-dimensional point processes. *Biometrika* **51** 299–311. MR0175254

[4] Burguet, J. and Andrey, P. (2014). Statistical comparison of spatial point patterns in biological imaging. *PLoS ONE* **9** e87759.
[5] Coates, D. S. and Diggle, P. J. (1986). Tests for comparing two estimated spectral densities. *J. Time Ser. Anal.* **7** 7–20. MR832349
[6] Crujeiras, R. M., Fernández-Casal, R. and González-Manteiga, W. (2007). Comparing spatial dependence structures using spectral density estimators. *Environmetrics* **18** 793–808. MR2408945
[7] Diggle, P. J. (1983). *Statistical analysis of spatial point patterns. Mathematics in Biology*. Academic Press, London. MR743593
[8] Diggle, P. J. (1985). Comparing estimated spectral densities using GLIM. In *Generalized Linear Models* 35–43. Springer.
[9] Diggle, P. J. and Fisher, N. I. (1991). Nonparametric comparison of cumulative periodograms. *J. Roy. Statist. Soc. Ser. C* **40** 423–434. MR1115571
[10] Dorai-Raj, S. S. (2001). *First- and second-order properties of spatiotemporal point processes in the space-time and frequency domains*. ProQuest LLC, Ann Arbor, MI, Thesis (Ph.D.)–Virginia Polytechnic Institute and State University. MR2708257
[11] Fan, J. and Zhang, W. (2004). Generalised likelihood ratio tests for spectral density. *Biometrika* **91** 195–209. MR2050469
[12] Fokianos, K. and Savvides, A. (2008). On comparing several spectral densities. *Technometrics* **50** 317–331. MR2528655
[13] Hahn, U. (2012). A studentized permutation test for the comparison of spatial point patterns. *J. Amer. Statist. Assoc.* **107** 754–764. MR2980082
[14] Jarrah, A., Nianga, J.-M., Iost, A., Guillemot, G. and Najjar, D. (2010). On the detection of corrosion pit interactions using two-dimensional spectral analysis. *Corrosion Sci.* **52** 303–313.
[15] Lund, R., Bassily, H. and Vidakovic, B. (2009). Testing equality of stationary autocovariances. *J. Time Series Anal.* **30** 332–348. MR2512238
[16] Mattfeldt, T., Eckel, S., Fleischer, F. and Schmidt, V. (2006). Statistical analysis of reduced pair correlation functions of capillaries in the prostate gland. *J. Microsc.* **223** 107–119. MR2247180
[17] Mattfeldt, T., Eckel, S., Fleischer, F. and Schmidt, V. (2007). Statistical modelling of the geometry of planar sections of prostatic capillaries on the basis of stationary Strauss hard-core processes. *J. Microsc.* **228** 272–281. MR2412516
[18] Møller, J. and Waagepetersen, R. P. (2004). *Statistical inference and simulation for spatial point processes*. Chapman & Hall/CRC, Boca Raton. MR2004226
[19] Mugglestone, M. A. and Renshaw, E. (1996a). The exploratory analysis of bivariate spatial point patterns using cross-spectra. *Environmetrics* **7** 361–377.
[20] Mugglestone, M. A. and Renshaw, E. (1996b). A practical guide to the spectral analysis of spatial point processes. *Comput. Statist. Data Anal.* **21** 43–65. MR1380832
[21] Myllymäki, M., Mrkvicka, T., Grabarnik, P., Seijo, H. and Hahn, U. (2013). Global envelope tests for spatial processes. *ArXiv e-prints*.
[22] Pagano, M. (1971). Some asymptotic properties of a two-dimensional periodogram. *J. Appl. Probab.* **8** 841–847. MR0292247
[23] Renshaw, E. and Ford, E. (1983). The interpretation of process from pattern using two-dimensional spectral analysis: Methods and problems of interpretation. *Appl. Stat.* 51–63.
[24] Renshaw, E. and Ford, E. (1984). The description of spatial pattern using two-dimensional spectral analysis. *Vegetatio* **56** 75–85.
[25] Robert, C. P. (2007). *The Bayesian choice*, second ed. *Springer Texts in Statistics*. Springer, New York, From decision-theoretic foundations to computational implementation. MR2723361
[26] Taheriyoun, A. R. (2012). Testing the covariance function of stationary Gaussian random fields. *Statist. Probab. Lett.* **82** 606–613. MR2887478

Azam Saadatjouy
Department of Statistics
Shahid Beheshti University
Evin, 1983969411
Tehran
Iran
E-mail address: a_saadatjouy@sbu.ac.ir

Ali Reza Taheriyoun
Department of Statistics
Shahid Beheshti University
Evin, 1983969411
Tehran
Iran
E-mail address: a_taheriyoun@sbu.ac.ir